Available online at www.sciencedirect.com
SCIENCE DIRECT®
Journal of Chromatography A, 1015 (2003) 205–218
JOURNAL OF CHROMATOGRAPHY A
www.elsevier.com/locate/chroma

Dispersion effects of laminar flow and spray chamber volume in capillary electrophoresis–inductively coupled plasma-mass spectrometry: a numerical and experimental approach

Jeroen E. Sonke [a,*], David Jon Furbish [b], Vincent J.M. Salters [a]

[a] *Geochemistry Division, National High Magnetic Field Laboratory, Department of Geological Sciences, Florida State University, Tallahassee, FL 32306, USA*
[b] *Department of Geological Sciences and Center for Earth Surface Processes Research, Florida State University, Tallahassee, FL 32306, USA*

Received 25 September 2002; received in revised form 9 July 2003; accepted 9 July 2003

Abstract

Band broadening related to laminar flow and spray chamber dead volume is a potential problem in flow injection (FI)–inductively coupled plasma-mass spectrometry (ICP-MS). We studied these two dispersion effects with a sheath flow capillary electrophoresis (CE)–ICP-MS interface. A numerical model was used to simulate advection diffusion processes in the CE-capillary and dispersion in the spray chamber. Experimental results of FI with this CE–ICP-MS interface agree well with numerical modeling results. Dispersion due to laminar flow depends strongly on capillary diameter and analyte diffusion coefficient and to a lesser extent on laminar velocity and capillary length and typically amounts to one order of magnitude peak width increase. Three spray chambers of 5, 20 and 150 ml dead volume showed an increase in band broadening and peak tailing with increasing dead volume. The use of standard Scott-type spray chambers (>90 ml volume) increases peak widths by 5–10 s regardless of injection time. The use of a low dead volume spray chamber is recommended for experiments where resolution is critical. The modeling approach can be extended to the coupling of other flow injection techniques, like micro-LC and nano-LC with ICP-MS.

Keywords: Dispersion; Laminar flow; Spray chamber; Numerical simulation; Flow injection; Inductively coupled plasma-mass spectrometry

1. Introduction

The coupling of chromatographic separation techniques to mass spectrometric detectors for speciation studies has seen a strong development over the last decade [1,2]. With respect to capillary electrophoresis, the capillary electrophoresis–inductively coupled plasma-mass spectrometry (CE–ICP-MS) interface design has mainly been guided by the requirement of closing the electrical (high voltage) CE circuit and providing a sufficient solute flow for nebulization. The so-called sheath-flow interface has proven to be particularly effective in coupling CE to a plasma source using a variety of nebulizer–spray chamber combinations [3–7]. Sheath-flow interfaces are based on inserting the CE capillary via a tee construction

* Corresponding author. Tel.: +1-850-644-2263; fax: +1-850-644-0827.
E-mail address: sonke@magnet.fsu.edu (J.E. Sonke).

0021-9673/$ – see front matter © 2003 Elsevier B.V. All rights reserved.
doi:10.1016/S0021-9673(03)01210-X

through the nebulizer central channel to the nebulizer tip. At the tip the nanoliter size flow from the CE capillary is combined with the microliter to milliliter size sheath flow. The sheath flow is either mechanically pumped to the nebulizer [5,7–12] or generated through self aspiration [4,6,13]; i.e. the nebulizer gas stream creates a negative pressure difference between sheath flow reservoir and nebulizer tip (Venturi effect) which results in siphoning of the sheath flow. Mechanical delivery of the sheath flow with peristaltic or syringe pumps facilitates more precise flow rate control, yet may introduce pump pulsation artifacts. With the tip of the CE capillary positioned at an arbitrary point between nebulizer tip and sheath flow reservoir (yet often close to the nebulizer tip), the CE flow combines with the sheath flow at a point where the dynamic fluid pressure corresponds to the pressure gradient set-up by the nebulizer gas. At this mixing point, the dynamic solution pressure is lower than the atmospheric pressure at the CE capillary inlet and a secondary siphoning flow inside the CE capillary is generated. The CE siphoning flow is laminar in nature and characterized by a parabolic, highly dispersive flow profile leading to band broadening of analyte peaks and thus a decrease in resolution. It has been established that the CE siphoning rate is inversely proportional to sheath flow rate with the possibility of tuning an experiment to '0' siphoning [5]. This follows from the fact an increased sheath flow that is mechanically pumped induces a shift in the dynamic pressure gradient (the sheath flow reservoir will have $P > P_{atm}$), thereby minimizing the pressure gradient over the CE capillary inlet which remains at P_{atm}. Others have found that reducing the capillary diameter to 20 μm [14] or optimizing the interface fluid dynamics [3,6] minimizes the negative pressure difference between CE capillary inlet and outlet and avoids the siphoning effect. However, the absence of siphoning requires pressurized injection of sample plugs, which can only be made by costly commercial CE devices.

CE experimentalists make use of pressurized laminar flow for other reasons, such as the detection of both positively and negatively charged species or the necessity of rapid elution times to monitor reaction kinetics in the sample vial [11,15]. The gain in versatility or analysis time is always at the cost of resolution. Whether laminar flow is induced by a negative pressure difference at the outlet of the capillary (siphoning) or a positive pressure at the inlet (pressurized flow), does not effect the underlying fluid dynamics and consequently its theoretical and numerical treatment.

An additional 'extra-column' factor of band broadening has been recognized in the spray chamber dead volume [13,14,16,17]. Large dead volumes or low transportation rates, i.e. nebulizer gas flow rate, result in prolonged residence times of analytes in the chamber. In conventional continuous detection of analytes this results usually in lower sensitivity and longer wash-out times, however these adverse effects are minimal compared to the benefits: effective droplet removal and signal stability enhancement. In chromatographic MS applications the detection of transient signals critically depends on the adverse effects: lower sensitivity and long wash-out times result in band broadening and peak tailing. The theoretical description of this process stems from the engineering concept of mixing chambers and has been fully treated for chromatographic applications by Sternberg [18]. Nevertheless, the theoretical basis is sparsely applied in a predictive model of spray chamber dispersion [16]. In the race for ultra high resolution, a number of direct injection nebulizers (DIN) have successfully been interfaced with CE capillaries [7,8,19]. Since no spray chamber is involved, there is no additional band broadening beyond the CE capillary. Although, potentially an ideal solution, DIN operation commonly results in higher oxide formation, lower sensitivity, higher LODs and higher cost. Therefore, we revisit the analysis of the spray chamber dispersive process considering that a CE–ICP-MS approach should focus on the minimum resolution required rather than the maximally attainable resolution [15].

Here we present the results of an experimental and theoretical study into the dispersion effects of laminar flow in the CE capillary, and spray chamber volume. We compare the experimentally determined peak shapes with a dynamic numerical model. The numerical simulations we present for siphoning and spray chamber dispersion are mathematically easily programmable. This allows the novice in numerical modeling to simulate and optimize their CE–ICP-MS interface with respect to maximally allowed band broadening. We emphasize that all experiments were performed without high voltage, in order to single out laminar flow dispersion.

2. Experimental

2.1. CE–ICP-MS interface

A sheath flow interface was used to introduce the CE eluent to a Glass Expansion 'micromist' nebulizer (100 μl min^{-1}), followed by ICP-MS detection (Fig. 1). A 10 ml BD plastic syringe contained the 1% HNO_3 sheath flow solution that was pumped by a syringe pump (Harvard Apparatus 22) at flow rates between 5–67 μl min^{-1} to a microcross (UpChurch Sci.; Oak Harbor, WA) that also guides the CE capillary and the ground electrode through the remaining three inlets. CE capillaries (50 μm I.D., 130 μm O.D.) were obtained from Polymicro Technologies (Phoenix, AZ) and cut at the approximate desirable length. Capillary tips were subsequently fine polished using diamond abrasive pads, using a custom made tool [20], until tips were perfectly crosscut.

Sample injection was automated using a six-port injection valve (Valco Instruments Co., Houston, TX), controlled by a Microneb 2000 control unit (CETAC, Omaha, NB). The capillary inlet was inserted through a second microcross (Fig. 1) and guided to the outlet of the injection valve through 500 μm I.D. (1/16 in. O.D.) PFA tubing. By choosing a capillary inlet position parallel to the solution flow and upstream of the microcross at the injection valve, dead volume problems could be prevented and ICP-MS detection timing synchronized with flow injection timing. Buffer and sample flow to the injection valve were supplied by a peristaltic pump at 120 μl min^{-1}. At the capillary inlet, the solution velocity was 1 cm s^{-1} and did not induce pressurized flow into the CE capillary over at least 30 min of visibly monitoring the capillary outlet. Rather, the siphoning effect at the outlet of the capillary draws solution from the main stream during full operation of the interface.

Three Teflon spray chambers, with internal volumes (including injector volume) of 6.1, 20.1 and 150 ml (5, 20 and 150 ml nominal) were used. The 5 and 150 ml chambers were build out of Teflon PFA unions, elbows segments and transfer caps (Savilex Corp.). The 20 ml chamber was custom machined out of Teflon. The 20 and 150 ml chambers have a Teflon baffle for more efficient droplet removal and all three chambers have a drain that is pumped by a peristaltic pump. Low

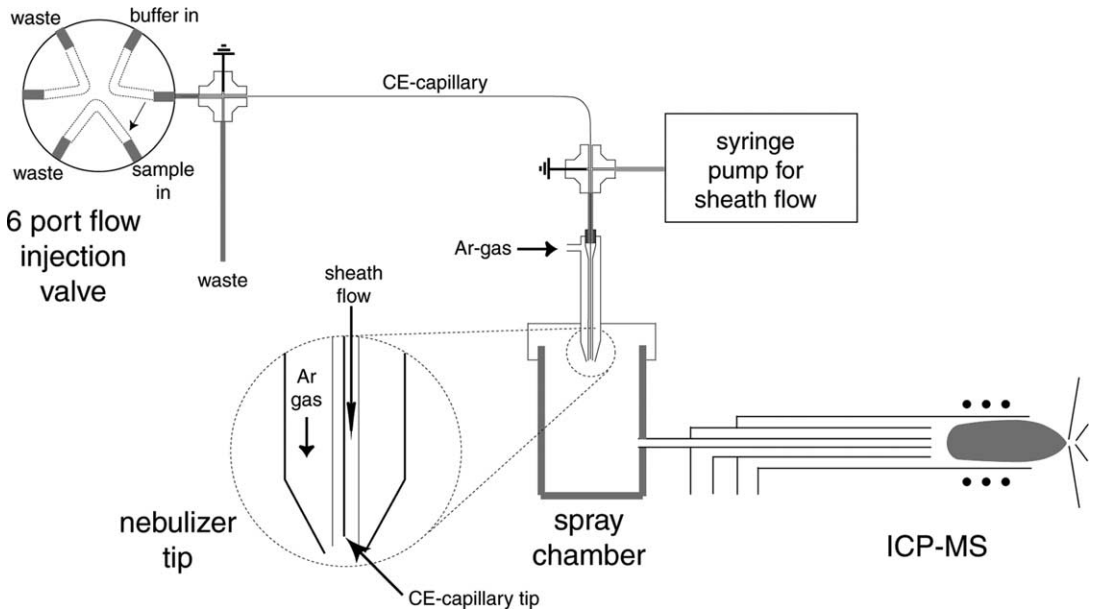

Fig. 1. CE–ICP-MS interface. A six port flow injection valve continuously delivers 'buffer' (1% HNO_3) and sample flow to a microcross that maintains the CE capillary parallel to the pumped solution flow. The CE capillary outlet is guided through a second microcross towards the tip of the nebulizer where it siphons into a sheath flow solution.

Table 1
Experimental conditions used for CE–ICP-MS

CE–ICP-MS interface	
Sheath flow rate	5–67 μl min^{-1}
Buffer/sample flow rate	120 μl min^{-1}
Capillary	Fused silica, 32–67.5 cm length, 50 μm I.D., 130 μm O.D.
"Buffer" solution	1% HNO_3, spiked with 1 ppb Ce
Sample solution	1% HNO_3, spiked with 1 ppb Nd
Sheath flow solution	1% HNO_3, spiked with 1 ppb Ba and In
ICP-MS	
Cool gas	13 l min^{-1}
Auxiliary gas	0.7–1.0 l min^{-1}
Nebulizer gas	1.09–1.18 l min^{-1}
Power	1250 W
Mass resolution	300
Scan duration	500 ms
Isotopes monitored	^{138}Ba, ^{140}Ce and ^{146}Nd
Sensitivity	
150 ml SC, 67 μl min^{-1} sheath flow	1 ppb In ∼ 850000 cps
150 ml SC, 10 μl min^{-1} sheath flow	1 ppb In ∼ 250000 cps
20 ml SC, 10 μl min^{-1} sheath flow	1 ppb In ∼ 150000 cps
5 ml SC, 10 μl min^{-1} sheath flow	1 ppb In ∼ 120000 cps

volume spray chambers do not handle high solvent loads well and therefore require a nebulizer that operates properly in the 5–20 μl min^{-1} (sheath) flow range. We performed most experiments at 10 μl min^{-1} without losing signal stability. Signal intensity does drop at lower flow rates and lower spray chamber volumes (Table 1).

A Finnigan Matt "ELEMENT", high-resolution magnetic sector ICP-MS was used as a mass specific detector. Operating conditions are given in Table 1. For transient signal detection we switched between masses for internal standards and analyte ^{138}Ba, ^{140}Ce and ^{146}Nd using electric scans (i.e. varying the accelerating voltage at constant magnetic field).

Elemental standards (10 ± 0.05 ppm Ce, Nd, Ba, In) were obtained from High Purity Standards Inc. Ba was added to the sheath flow solution at a 1 ppb concentration, Ce was added to the buffer solution at a 1 ppb concentration and Nd was added to the sample solution at a 1 ppb concentration (∼7 nM). The band broadening effects were studied without applying high voltage, as Joule heating and EOF may add additional dispersive factors.

2.2. Theory

In order to simulate a siphoning experiment numerically, we need to consider longitudinal diffusion and advection of the analyte of interest. The corresponding transport equation is the advection diffusion equation, here given in one dimension:

$$\frac{dc}{dt} = D\frac{d^2c}{dx^2} - u_{siph}\frac{dc}{dx} \quad (1)$$

where c is the cross-sectional averaged concentration of analyte (mol kg^{-1}), u_{siph} is the average siphon rate (advective velocity, (m s^{-1})) and D is the analyte diffusion coefficient (m^2 s^{-1}). D was calculated via the Nernst–Einstein relationship [21] with a limiting ionic mobility for Nd^{3+} of $6.94 \cdot 10^{-3}$ m^2 V^{-1} S s^{-1} [22]. We apply Taylor's analysis of parabolic flow to derive a dispersion coefficient, K, from the diffusion coefficient D, allowing for a one dimensional simulation, which is inherently simpler for describing advective flow [23,24] (see Appendix A):

$$K = \frac{a^2(2u_{siph})^2}{192D} \quad (2)$$

where a is the capillary radius (m). Additivity of dispersion by longitudinal molecular diffusion and parabolic flow then allows addition of K to D in Eq. (1) [25]. The sum of K and D will be referred to as 'total dispersion coefficient'. We note that in the plate height model of band broadening, the total dispersion coefficient is described by the Golay equation which is partly derived from Eq. (2) [26].

Since we apply no voltage and use an acid matrix, dispersion effects due to Joule heating and wall adsorption can be omitted. Concentration overload can be neglected based on the plate height model [21]. Dispersion from siphoning injection of the sample is included in the model. The limiting ionic mobility of analyte Nd^{3+}, that determines D is not corrected for the acid ionic strength (1% HNO_3) due to lack of an appropriate correction model. Based on successful results (i.e. in hindsight) we expect this correction term to be insignificant.

2.3. Numerical modeling

2.3.1. Capillary Dispersion Model (C-DM)

In order to find the numerical solution to the partial differential equation (PDE, Eq. (1)), we use a finite-difference method that replaces the partial derivatives by finite difference approximations. Various explicit (i.e. solving the concentration profile at '$t + \mathrm{d}t$', based on the concentration profile at 't') finite difference schemes (FDS) can be used [27–29], however not all yield a stable solution of the PDE. In keeping the math as simple as possible we used an explicit approximation for Eq. (1); forward time backward space (FTBS) approximation for the first derivative (advection) and a forward time central space (FTCS) approximation for the second derivative (diffusion) [30]:

$$\frac{c_x^{t+\mathrm{d}t} - c_x^t}{\mathrm{d}t} = -u_{\mathrm{siph}} \frac{(c_{x+\mathrm{d}x}^t - c_x^t)}{\mathrm{d}x} + (D + K) \frac{(c_{x+\mathrm{d}x}^t - 2c_x^t + c_{x-\mathrm{d}x}^t)}{(\mathrm{d}x)^2} \quad (3)$$

which is solved for $c_x^{t+\mathrm{d}t}$ given a set of starting and boundary conditions. We forced the advective FDS scheme to operate under the Courant–Fredrichs-Levy (CFL) condition of 1 by choosing $\mathrm{d}t = 0.1\,\mathrm{s}$ and subsequently fixing $\mathrm{d}x = u_{\mathrm{siph}}\mathrm{d}t$ (see Appendix A) as a function of siphoning rate u_{siph} ($\mathrm{cm\,s^{-1}}$). This typically yields a least 1000 time and 1000 spatial steps to model one experiment. The results can be viewed as a concentration distribution over the capillary length at a certain time, or as an elution profile at the outlet of the capillary, i.e. concentrations as a function of time (electropherogram). The latter is referred to as Capillary Dispersion Model (C-DM) in Section 3.

2.3.2. Capillary Spray Chamber-Disperion Model (CSC-DM)

In order to model the dispersion effect of the spray chamber, we used the C-DM output in the form of concentration as a function of time at the capillary outlet. The shape of the detected transient signal, $N_{\mathrm{ICP}}(t)$, depends both on the eluted temporal profile as well as on the exponential decay caused by analyte dilution within the spray chamber. We will use the concept of an ideal mixing chamber [18] to model spray chamber dilution, as has been applied successfully by others [16,31]. The results for $N_{\mathrm{ICP}}(t)$ will be referred to as CSC-DM. We will outline a computational approach based on mass balancing spray chamber input and output that allows an easy programmable finite difference approximation.

For simplification purposes we assume that the amount of analyte ions, N_0 (mol), that elutes from the capillary during time step, dt, is diluted by the sheath flow (with density, ρ_{liq} ($\mathrm{kg\,m^{-3}}$)) by a factor 'ϕ' (ratio of CE flow rate to sheath flow rate) and subsequently transferred into a volume of nebulizer gas (V_{gas}), that flows at Q_{neb} ($\mathrm{l\,s^{-1}}$) into the SC (with volume V_{SC} (l)), and can thus be expressed in units of moles per volume of gas:

$$C_0 = \frac{c_{x=L}^t \times u_{\mathrm{siph}}\mathrm{d}t \times \pi a^2 \times \rho_{\mathrm{liq}} \times \varphi}{Q_{\mathrm{neb}}\mathrm{d}t} \quad (4)$$

We emphasize that the concept of an ideal mixing chamber is based on uniform mixing of each volume of gas that enters the chamber volume, such that the exiting gas is always at the composition of the gas in the chamber, $C_{\mathrm{ICP}} = C_{\mathrm{SC}}$. Then by definition the rates of change per unit time are:

$$\frac{\mathrm{d}C_{\mathrm{ICP}}}{\mathrm{d}t} = \frac{\mathrm{d}C_{\mathrm{SC}}}{\mathrm{d}t} \quad (5)$$

During time step, dt, the change in the amount of analyte ions in the chamber, dN_{c} (mol), is the difference between the amounts that enter and leave the chamber:

$$\mathrm{d}N_{\mathrm{SC}} = N_0 - N_{\mathrm{ICP}} \quad (6)$$

By writing the mixing chamber constants V_{SC} and Q_{neb} explicitly,

$$V_{\mathrm{SC}} \times \mathrm{d}C_{\mathrm{SC}} = Q_{\mathrm{neb}}(C_0 - C_{\mathrm{ICP}})\,\mathrm{d}t \quad (7)$$

and rearranging and inserting Eq. (5),

$$\frac{\mathrm{d}C_{\mathrm{ICP}}}{\mathrm{d}t} = \frac{Q_{\mathrm{neb}}}{V_{\mathrm{SC}}}(C_0 - C_{\mathrm{ICP}}) \quad (8)$$

The change in spray chamber output, dC_{ICP}/dt, has now been expressed as a function of input and output and the characteristic constants Q_{neb} and V_{SC}, without the need of knowing C_{SC} or dC_{SC}/dt. Using a forward time approximation and substituting, $\tau = V_{\mathrm{SC}}/Q_{\mathrm{neb}}$, we obtain the following FDS that can be solved for $C_{\mathrm{ICP}}(t + \mathrm{d}t)$ given a set of initial conditions at time t:

$$\frac{C_{\mathrm{ICP}}^{t+\mathrm{d}t} - C_{\mathrm{ICP}}^t}{\mathrm{d}t} = \frac{1}{\tau}(C_0^t - C_{\mathrm{ICP}}^t) \quad (9)$$

By letting this FDS operates on the same time scale as the C-DM the two schemes can be coupled by updating C_0^t in Eq. (9) every time step, dt, by C_0 from Eq. (4). Because spray chamber transmission is typically less than 100%, an efficiency factor 'ε_N' could be introduced [32] by writing $\varepsilon_N C_0^t$ in Eq. (9). However, transmission loss is beyond the scope of this study and does not affect transient peak shape. Therefore, we omit the factor ε_N in our computational approach.

It is worth mentioning that the analytical solution to Eq. (8) is extensively applied in time-series analysis [33] and is of the form:

$$C_{\mathrm{ICP}}(t) = \int_0^\infty v(u) \times C_0(t-u)\,\mathrm{d}u \tag{10}$$

where $C_0(t)$ can be any arbitrary input function and the impulse response function $v(u) = \mathrm{e}^{(-t/\tau)}$ describes the exponential decay inside the mixing chamber. The output function then becomes:

$$C_{\mathrm{ICP}}(t) = \left\{\int_0^1 e^{-t/\tau}\right\} C_0(t-1) + \left\{\int_1^2 e^{-t/\tau}\right\} \times C_0(t-2) + \cdots \tag{11}$$

which requires a method of bookkeeping that keeps track of the exponential decay of every amount C_0 that eluted into the SC at all past time steps and is far more computationally expensive and complex than the finite difference expression (Eq. (9)).

3. Results and discussion

Siphoning rates were determined for each individual injection series from the elution time of the first peak and monitored with the buffer internal standard (Ce) during an experiment. The reproducibility of the flow injection loading technique is shown in Fig. 2 for ten consecutive 5 s, three 10 s and one 60 s injection. The peak area reproducibility is ~1% R.S.D. for the ten 5 s injections as well as the three 10 s injections. The influence of band broadening is shown by the respective 52 and 22% decrease in peak height of the 5 and 10 s injections relative to the plateau intensity of the 60 s injection. Additionally strong peak tailing is present and characteristic of the 150 ml spray chamber.

Dispersion experiments were conducted by triplicate flow injections of 1, 3, 5, 10, 15, 20, 25, 30 and 60 s, while varying capillary length, L, siphoning rate, u_{siph}, and spray chamber volume, V_{spray}. Siphoning rate was varied both by changing the sheath flow rate and by lifting or lowering the capillary inlet relative

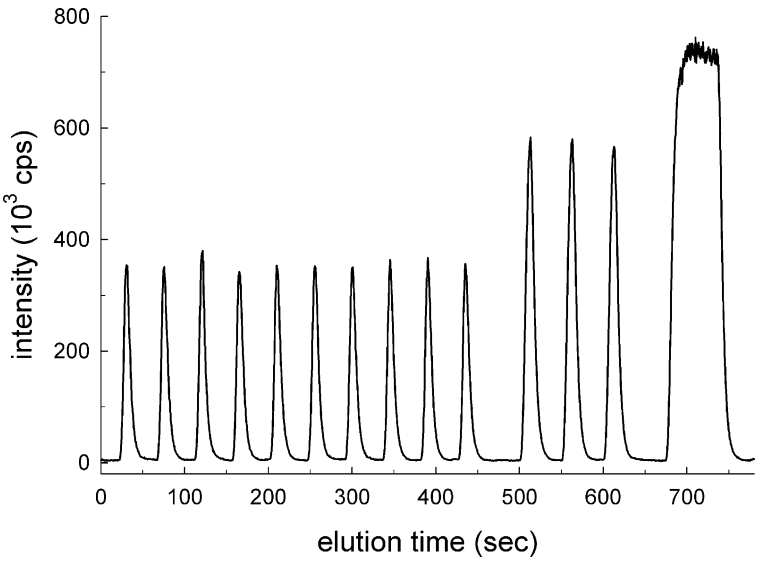

Fig. 2. Flow-injection of ten 5 s, three 10 s and one 60 s samples yield peak area reproducibilities of 1.0% R.S.D. Experimental conditions: L_{cap} is 32.0 cm, V_{SC} is 146 ml, u_{siph} is 0.11 cm s^{-1}, 1 ppb indium (8.7 nM) in 1% HNO_3.

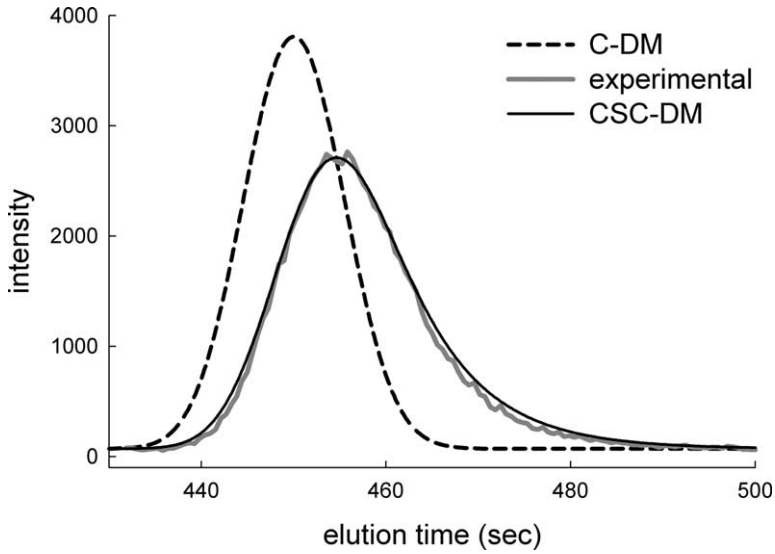

Fig. 3. Elution profiles of an experimental vs. a modeled 10 s injection. Experimental conditions: V_{SC} is 0.146 l, L_{cap} is 67.5 cm, u_{siph} is 0.152 cm s^{-1}, u_{gas} is 1.18 l min^{-1}. Intensity units are arbitrary as experimental peak height is matched with CSC-DM peak height due to omission of transmission loss factor in the CSC-DM.

to the fixed outlet. Peak widths of the eluted profiles as well as simulated profiles were determined by the 'tangent' method. Additionally the W_{10} (peak width at 10% of peak height) and peak asymmetry [34] were used to evaluate skewed peak shapes due to large spray chamber volumes.

Fig. 3 shows the simulation capabilities in a direct comparison with an experimental injection that starts

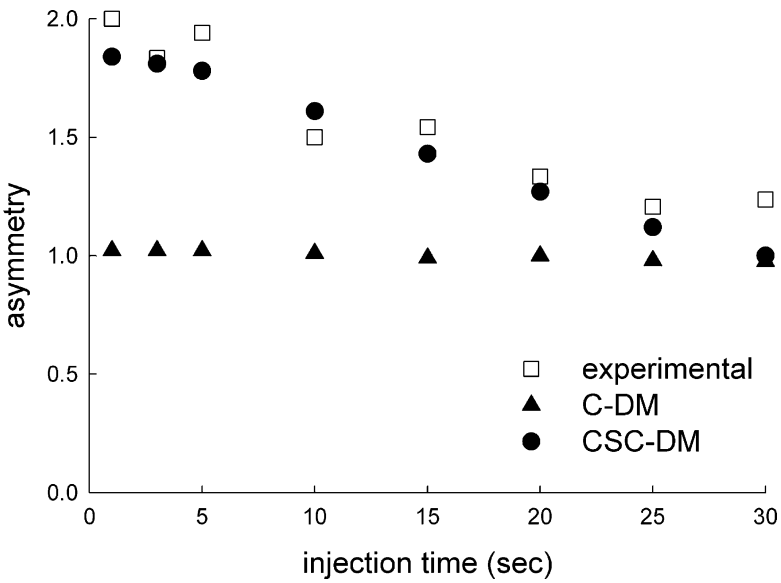

Fig. 4. Peak asymmetry as a function of injection time. Experimental conditions: V_{SC} is 0.146 l, L_{cap} is 67.5 cm, u_{siph} is 0.152 cm s^{-1}, u_{gas} is 1.18 l min^{-1}. Spray chamber mixing is the major contributor to peak asymmetry 'tailing'.

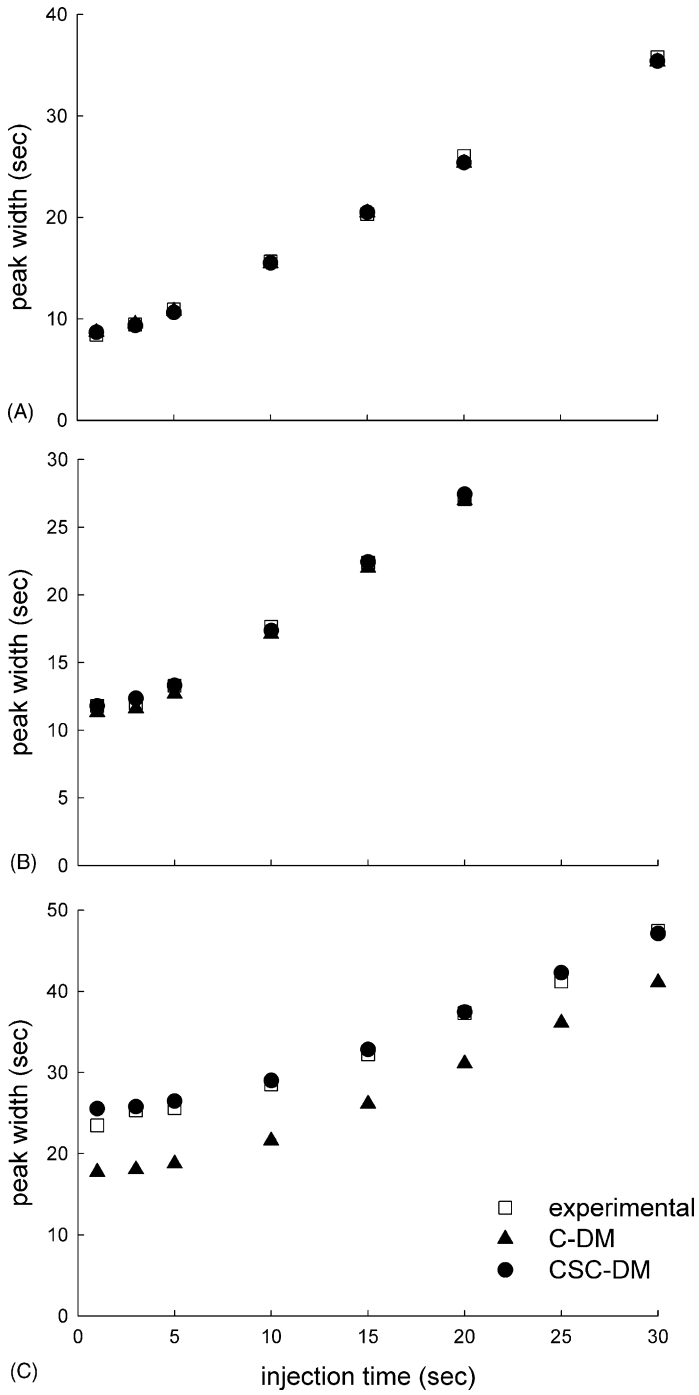

Fig. 5. Experimental and simulated peak widths as a function of injection time and spray chamber volume. Experimental conditions: (A) V_{SC} is 0.150 l, L_{cap} is 67.5 cm, u_{siph} is 0.152 cm s^{-1}, u_{gas} is 1.18 l min^{-1}, (B) V_{spray} is 0.0209 l, L_{cap} is 32.0 cm, u_{siph} is 0.181 cm s^{-1}, u_{gas} is 1.09 l min^{-1}; (C) V_{spray} is 0.0061 l, L_{cap} is 32.0 cm, u_{siph} is 0.294 cm s^{-1}, u_{gas} is 1.14 l min^{-1}. Analyte is 7 nM Nd in 1% HNO_3 under all conditions.

as a near rectangular 10 s plug. The peak shape of the sample plug eluting into the spray chamber is Gaussian while the peak shape after passing through the spray chamber is tailed on right hand side and shows retardation of the peak maximum by 7 s. This retardation time is independent of chromatographic processes and solely a feature of spray chamber mixing. Therefore, when fingerprinting analyte peaks or experimentally determining mobilities, with any of the coupled FI–mass spectrometric techniques one has to correct the elution time for this retardation; i.e. using a 150 ml spray chamber after a 70 s chromatographic separation requires a 10% correction of elution times.

Peak skewedness is mainly caused by spray chamber mixing, as can be observed in Fig. 4 where experimental asymmetry is compared to simulated asymmetry as a function of injection time when (a) the analyte elutes from the capillary (C-DM) and (b) the analyte leaves the spray chamber (detection; CSC-DM).

A summary of experimental and simulated injection results are shown in Fig. 5A–C for respectively

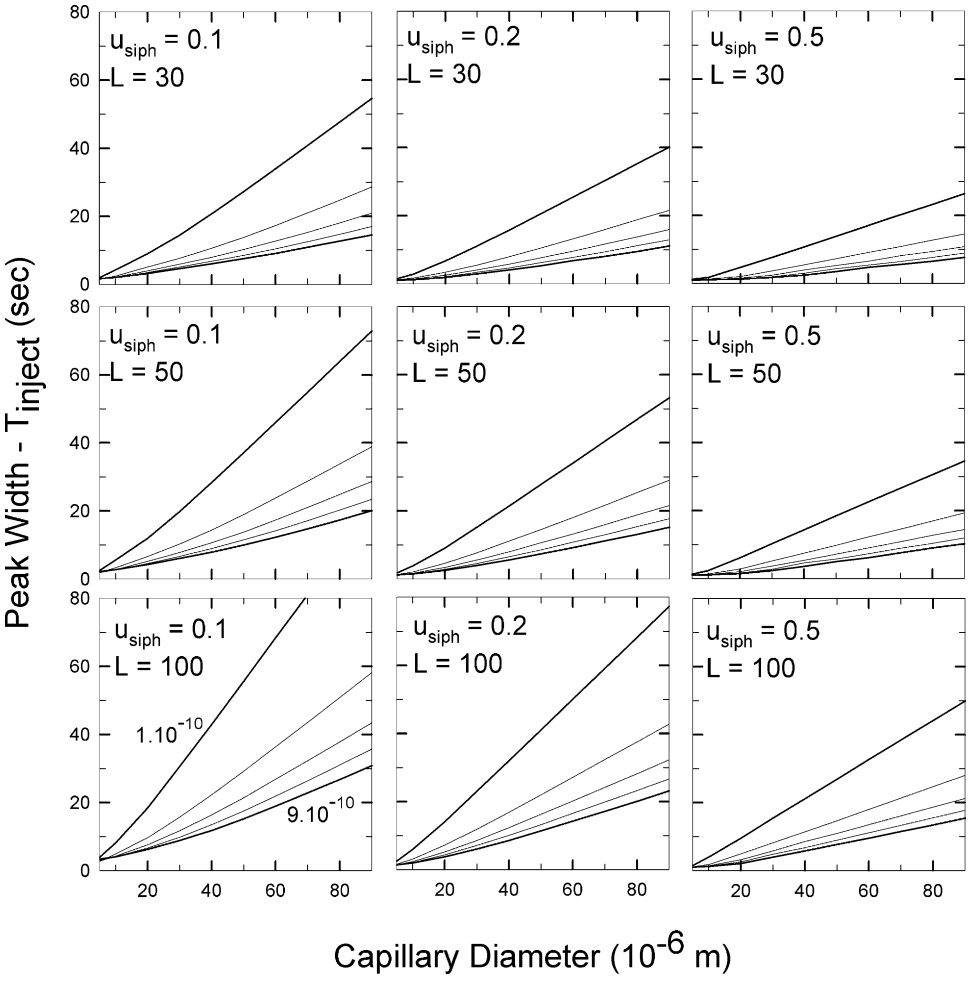

Fig. 6. Simulated increase in peak width ($W - t_{inj}$) due to laminar flow, as a function of capillary diameter (5–90 μm), diffusion coefficient (1×10^{-10}, 3×10^{-10}, 5×10^{-10}, 7×10^{-10} and 9×10^{-10} $m^2\ s^{-1}$), laminar flow velocity, u_{siph}, (0.1, 0.2, 0.5 cm s^{-1}) and capillary length, L, (cm). Sample injection in all simulations is 1 cm of capillary length, corresponding to 10, 5 and 1 s injections for the respective u_{siph} of 0.1, 0.2 and 0.5 cm s^{-1}. Variation as a function of diffusion coefficient is represented by the five separate curves within one plot; the lower left plot indicates actual values.

the 150, 20 and 5 ml spray chambers. Experimental peak widths increased by a factor 9–25 for 1 s injections and a factor 1.6–9 for 10 s injections. The C-DM model explains the entire experimental band broadening for the 6 and 20 ml spray chambers, whereas the CSC-DM model adds minimal dispersion effects due to spray chamber mixing (Fig. 5B and C). However, for the 150 ml spray chamber the CSC-DM model comprises an additional 30–40% of the observed peak width increase (Fig. 5A). Similar results to Fig. 5 with

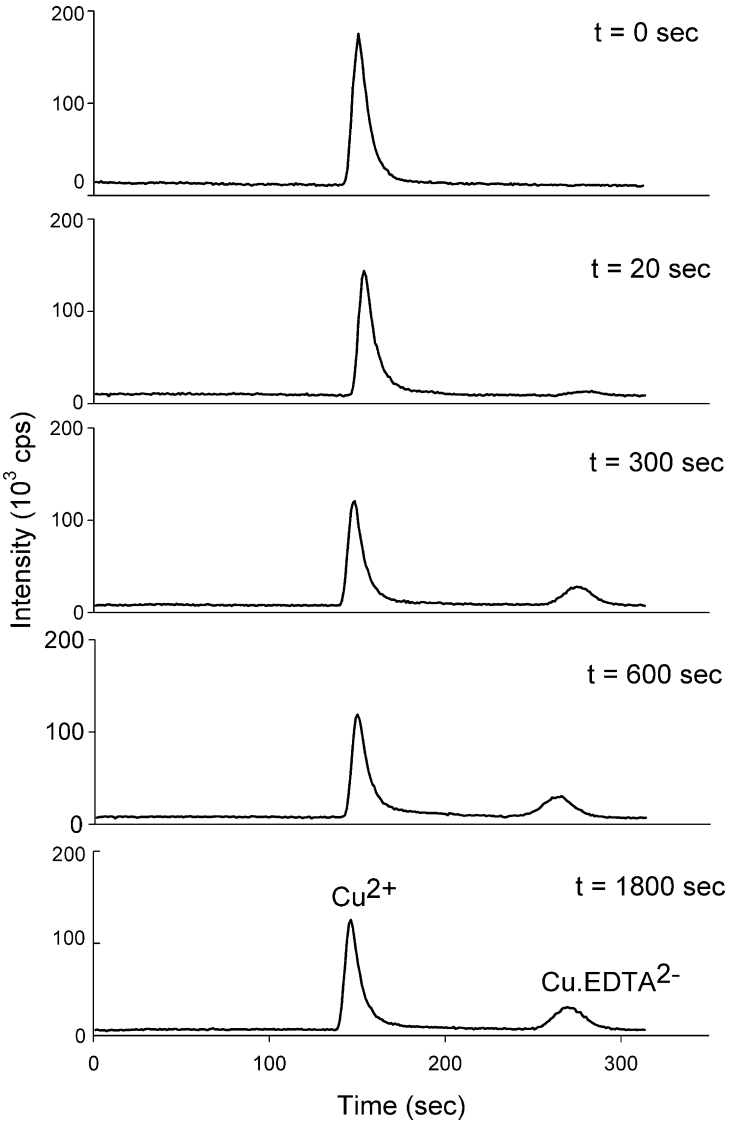

Fig. 7. Series of CE separations of Cu^{2+} and Cu–$EDTA^{2-}$ complexes. Siphoning was used to load sample (10 s), elute both positive and negative complexes, and speed up the separation to track a kinetic experiment of Cu–EDTA binding, inhibited by Zn–$EDTA^{2-}$ dissociation. Separation conditions: L_{cap} is 45 cm, capillary I.D.: 50 μm, 12.5 kV separation voltage, u_{siph} is 0.16 cm s^{-1}, V_{SC} is 146 ml. Buffer: 10 mM $ZnSO_4$ at pH 4.7. Sample: pre-equilibrated solution of 10 mM $ZnSO_4$ and 5 μM of Na_2H_2EDTA (at pH 4.7) to which 10 μM $CuSO_4$ was added at $t = 0$ s. Initially, all EDTA sites are occupied by Zn^{2+}, however due to the higher affinity of Cu for EDTA compared to Zn, a metal exchange reaction takes place which is kinetically limited by Zn–EDTA dissociation. By measuring the speciation of Cu as a function of time the Zn–Cu exchange can be quantified.

matching numerical simulations were obtained when varying siphoning rates by 50%.

3.1. Generalized modeling

Based on the excellent agreement between experimental and numerical results outlined above, we extended the numerical models for laminar flow and spray chamber dispersion to explore the parameter space beyond our experimental values. Laminar flow dispersion is a function of L, $D_i + K_i$, diameter, u_{siph}, and t_{inj}. In order to capture most of the variation in a presentable format we varied the most influential parameters, D_i and diameter continuously for a limited set of L and u_{siph}. We varied t_{inj} in such a way that each simulation is based on a '1 cm' sample plug. Instead of expressing the results as 'absolute peak width', W, or dispersion factor (W/t_{inj}), we plot the observed increase in peak width ($W - t_{inj}$ (s)) at the end of the capillary (Fig. 6). This makes the simulations relatively independent of t_{inj} and the results (Fig. 6) are valid within 20% uncertainty for sample plugs > 0.5 cm (1% of l) wide due to similar diffusion fronts. For sample plugs smaller than ~1% of the capillary length, separate simulations need to be performed. Fig. 6 clearly indicates the strong dependence of dispersion on ($D_i + K_i$): the smaller D_i, the larger K_i (Eq. (2)) and thus the larger laminar flow dispersion will be. This is an important negative feedback process with respect to CE–ICP-MS separation studies in the biochemical field. Analytes with low electrophoretic mobilities (and thus low D's), e.g. proteins, require more time to separate, yet at the same time suffer from the largest laminar flow dispersion; reducing if not avoiding laminar flow seems a necessity. Separation of analytes with larger differential electrophoretic

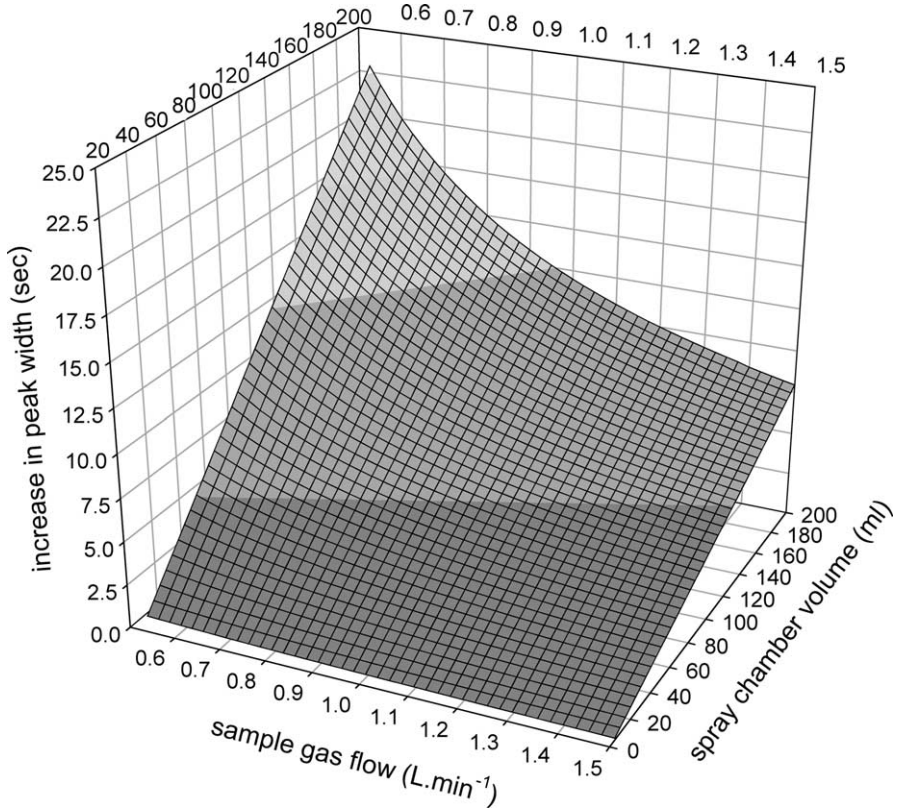

Fig. 8. Simulated increase in peak width ($W - t_{inj}$) due to spray chamber mixing, as a function of chamber volume (5–200 ml) and nebulizer gas velocity (0.5–1.5 l min^{-1}). The increase in peak width in the spray chamber is not a function of peak width and shape at capillary outlet and therefore plotted as the absolute value.

mobilities will result in less pronounced dispersion and laminar flow can be used as an advantage. Fig. 7 illustrates the latter in a series of rapid consecutive CE separations of a Cu–Zn–EDTA mixture, where siphoning has been used to detect both positively (Cu^{2+}) and negatively ($Cu–EDTA^{2-}$) charged species and to speed up the separation in order to monitor speciation changes over time (see caption for details).

Fig. 8 shows spray chamber dispersion as a function of V_{SC} and Q_{neb}. Dispersion is again expressed as the 'increase in W' as this is independent of the shape and peak width of the initial plug eluting from the capillary into the spray chamber. So whether a 1 s rectangular plug or a 25 s Gaussian plug enters the spray chamber, the increase in peak width for $V_{SC} = 0.1$ l and $Q_{neb} = 1.0\,l\,min^{-1}$ will be ~6 s. The conclusion to be drawn from Fig. 8 is straightforward in the sense that any chromatographic technique coupled to an ICP-MS will benefit from lower spray chamber volumes. However, as we observed a decrease in sensitivity with volume as well (Table 1), it may be worth to sacrifice some resolution for sensitivity and choosing a larger spray chamber when analyzing low-level speciation as in Fig. 7 (V_{SC} is 150 ml).

4. Conclusions

Experimental and numerical results on laminar flow and spray chamber dispersion indicate potential order of magnitude increases in peak width. Analyte diffusion coefficient and capillary diameter were identified as the main causes, while laminar flow velocity, capillary length and spray chamber volume are less, but significantly, influential. Our numerical framework and generalized results provide for optimization of separation resolution versus sensitivity and separation speed in those experiments where a trade-off can be made between analysis time, sensitivity and resolution. For experiments where resolution is critical, a reduction of spray chamber volume to less than 20 ml is strongly recommended. Because of the large number of experimental parameters involved in finding the optimum resolution of a CE–ICP-MS experiment, we find that an exploration of parameter space through simulations is an excellent complementary analysis tool in the development of chromatography–mass spectrometry interfaces.

5. Nomenclature

A	radius of the capillary (m)
C_0	initial concentration of analyte in the spray chamber (mol $(l_{gas})^{-1}$)
C-DM	Capillary Dispersion Model
C_{ICP}	concentration of analyte in the SC outflow gas (mol $(l_{gas})^{-1}$)
C_{SC}	concentration of analyte in the SC gas (mol $(l_{gas})^{-1}$)
CSC-DM	Capillary Spray Chamber-Disperion Model
c_x^t	molal concentration of analyte at grid point x, at time t (mol kg^{-1})
D	diffusion coefficient of analyte ($m^2\,s^{-1}$)
dt	time step of the numerical model (s)
dx	length step of the numerical model (m)
K	dispersion coefficient of analyte ($m^2\,s^{-1}$)
L_{cap}	length of capillary (m)
N_0	number of analyte ions that enter the SC (mol)
N_{ICP}	number of analyte ions that leave the SC (mol)
N_{SC}	number of analyte ions in the SC at time t (mol)
Q_{neb}	nebulizer gas flow ($l\,s^{-1}$)
r	radial distance, away from r_0 (m)
r_0	center of capillary (m)
SC	spray chamber
t_{ini}	initialization time for parabolic flow (s)
u_0	maximum velocity at r_0 (center axis) ($m\,s^{-1}$)
u_{gas}	nebulizer gas velocity (central channel) ($m\,s^{-1}$)
u_{siph}	average siphoning velocity ($m\,s^{-1}$)
V_{SC}	spray chamber volume (l)
W_{10}	peak width determined at 10% of the maximum value (s)
x	distance along the capillary (m)

Greek letters

ϕ	ratio of CE flow to sheath flow rates
ρ_{liq}	density of sheath flow solution ($kg\,m^{-3}$)
τ	spray chamber residence time (s)

Acknowledgements

This work was supported by a Cornerstone University Program Enhancement Grant from the Florida State University. Mark Schmeeckle and Sergio Fagherazzi are thanked for discussion, John Quinn is thanked for assistance with capillary polishing and Mark Emmett is thanked for loaning us a syringe pump. Comments from two anonymous reviewers helped improve the manuscript.

Appendix A.

A.1. Taylor's analysis

The velocity distribution of a parabolic flow profile as a function of radial distance r (m) is:

$$u(r) = u_0 \left(\frac{1 - r^2}{a^2} \right) \tag{A.1}$$

where a is the radius of the tube (m) and u_0 the maximum velocity ($m\,s^{-1}$) on the centerline. The mean velocity, u_{siph} is $u_0/2$. Taylor [23] showed that the parabolic concentration profile is established by a simple balance between longitudinal advective transport (varying along the radius) and cross-sectional diffusive transport. This led him to the derivation of Eq. (2) where the dispersion coefficient is inversely proportional to the molecular diffusion coefficient. This becomes clear when analyzing the balance described above; a large value of D will counteract the dispersion caused by rapid analyte advection along the centerline of the tube (u_{max}). The, larger the values of D, the more rapidly analyte will diffuse from the centerline to the wall where advective speeds are low. In essence, cross-sectional diffusion is a negative feedback to advective dispersion along the centerline. One limitation of Eq. (2) is that during a certain initialization time, t_{ini} (s), formulated as:

$$t_{ini} = \frac{0.4a^2}{D} \tag{A.2}$$

the above mentioned balance between advection and diffusion is not established yet, thereby inhibiting the validity of Eq. (2). However, for the range of parameters used to create Fig. 6, $t_{ini} < 5\%$ of the elution time and therefore insignificant.

A.2. FDS schemes

To obtain a stable solution for advective problems in general requires the use of implicit methods (i.e. solving the concentration profile at $t = t + dt$, based on the concentration profile at $t = t + dt$ simultaneously at all grid points), involving recasting the FDS into a matrix form and using advanced algorithms (e.g. Crank–Nicholson). The numerical stability criterion (CFL) for advection, approximated by the explicit FTBS scheme [35] is defined as:

$$\frac{u_{siph}\,dt}{dx} \leq 1 \tag{A.3}$$

Although the advective FTBS is stable when CFL < 1 simulations show that pure numerical advection (no diffusion or dispersion) of a rectangular plug always results in a Gaussian elution profile. This is the result of an artificial diffusion term, which is introduced when CFL < 1 and adds significant unwanted bias to the simulation. The FTBS scheme works optimally when CFL $= 1$, yielding perfect numerical advection. However this constraint seriously delimits the applicability of this scheme in general. For our purpose we can, however, sacrifice one degree of freedom (dx), by only allowing a choice for dt and setting $dx = u_{siph}dt$. This forces the advective FDS to operate under CFL $=$ 1 at any time, thereby avoiding computational bias. It is worth mentioning that when dispersion is not simulated in 1D but in 2D using Eq. (A.1) to describe the radial velocity as a function of radius, $u(r)$, this approach does not work. The variation in $u(r)$ will cause CFL $\neq 1$ and a solution can only be obtained by resorting to more complex explicit, such as Lax–Wendroff or to implicit finite difference schemes [35].

The numerical stability criterion for diffusion [35] is:

$$2\frac{(D_i + K_i)\,dt}{(dx)^2} \leq 1 \tag{A.4}$$

which was met for all experimental simulations.

References

[1] K. Sutton, R.M.C. Sutton, J.A. Caruso, J. Chromatogr. A 789 (1997) 85.
[2] R.M. Barnes, J. Fres, Anal. Chem. 361 (1998) 246.

[3] B. Michalke, P. Schramel, J. Chromatogr. A 750 (1996) 51.
[4] G.H. Lu, S.M. Bird, R.M. Barnes, Anal. Chem. 67 (1995) 2949.
[5] J.A. Kinzer, J.W. Olesik, S.V. Olesik, Anal. Chem. 68 (1996) 3250.
[6] D. Schaumloffel, A. Prange, J. Fres, Anal. Chem. 364 (1999) 452.
[7] Y. Liu, V. Lopezavila, J.J. Zhu, D.R. Wiederin, W.F. Beckert, Anal. Chem. 67 (1995) 2020.
[8] A. Tangen, W. Lund, B. Josefsson, H. Borg, J. Chromatogr. A 826 (1998) 87.
[9] V. Majidi, N.J. Miller-Ihli, Analyst 123 (1998) 809.
[10] K.L. Sutton, C. B'Hymer, J.A. Caruso, J. Anal. Atomic Spectrosc. 13 (1998) 885.
[11] I.I. Stewart, J.W. Olesik, J. Chromatogr. A 872 (2000) 227.
[12] M. Van Holderbeke, Y.N. Zhao, F. Vanhaecke, L. Moens, R. Dams, P. Sandra, J. Anal. Atomic Spectrosc. 14 (1999) 229.
[13] J.A. Day, K.L. Sutton, R.S. Soman, J.A. Caruso, Analyst 125 (2000) 819.
[14] A. Tangen, W. Lund, J. Chromatogr. A 891 (2000) 129.
[15] J.W. Olesik, J.A. Kinzer, E.J. Grunwald, K.K. Thaxton, S.V. Olesik, Spectrochim. Acta B: Atomic Spectrosc. 53 (1998) 239.
[16] B.W. Pack, S.J. Ray, R.A. Potyrailo, G.M. Hieftje, Appl. Spectrosc. 52 (1998) 1515.
[17] B.L. Sharp, J. Anal. Atomic Spectrosc. 3 (1988) 939.
[18] J.C. Sternberg, in: J.C. Giddings, R.A. Keller (Eds.), Advances in Chromatography, vol. 2, Marcel Dekker, New York, 1966.
[19] L. Bendahl, B. Gammelgaard, O. Jons, O. Farver, S.H. Hansen, J. Anal. Atomic Spectrosc. 16 (2001) 38.
[20] J.P. Quinn, M.R. Emmett, A.G. Marshall, A device for fabrication of emitters for low-flow electrospray ionization, 46th American Society for Mass Spectrometry (ASMS) Meeting, Orlando, FL, May 31–June 4, 1998.
[21] M.G. Khaledi, editor, High-performance capillary electrophoresis: theory, techniques and applications, John Wiley & Sons, New York, 1998, p. 1047.
[22] R.C. Weast, Handbook of Chemistry and Physics, The Chemical Rubber Co., Cleveland, 1999.
[23] G.I. Taylor, Proc. R. Soc. Lond. A 219 (1953) 186.
[24] H.B. Fischer, Mixing in Inland and Coastal Waters, Academic Press, New York, 1979.
[25] R. Aris, Proc. R. Soc. Lond. A 235 (1956) 67.
[26] C.F. Poole, S.K. Poole, Chromatography Today, Elsevier, Amsterdam, 1991.
[27] C. Schwer, B. Gas, F. Lottspeich, E. Kenndler, Anal. Chem. 65 (1993) 2108.
[28] J. Martens, J.C. Reijenga, J. Boonkkamp, R.M.M. Mattheij, F.M. Everaerts, J. Chromatogr. A 772 (1997) 49.
[29] R.A. Mosher, D.A. Saville, W. Thormann, The Dynamics of Electrophoresis, VCH Verlagsgesellschaft mbH, Weinheim, F.R.G., 1992.
[30] D.A. Anderson, J.C. Tannehill, R.H. Pletcher, Computational Fluid Mechanics and Heat Transfer, McGraw-Hill, 1984.
[31] J.F. Tyson, Anal. Chim. Acta 214 (1988) 57.
[32] Y.P. Hu, Z.X. Zhang, J. Zheng, J. Anal. Atomic Spectrosc. 9 (1994) 701.
[33] G.E.P. Box, G.M. Jenkins, Time Series Analysis: Forecasting and Control, Holden-Day Inc., San Fransisco, 1976.
[34] J.P. Foley, J.G. Dorsey, Anal. Chem. 55 (1983) 730.
[35] W.H. Press, S.A. Teukolsky, W.T. Vetterling, B.P. Flannery, Numerical Recipes in Fortran 77, Cambridge University Press, Cambridge, 1986 (http://www.library.cornell.edu/nr/bookfpdf.html).